BIOCHEMISTRY
including biophysical chemistry & molecular biology

Article

pubs.acs.org/biochemistry

UV Resonance Raman Spectroscopy Monitors Polyglutamine Backbone and Side Chain Hydrogen Bonding and Fibrillization

Kan Xiong,[†] David Punihaole, and Sanford A. Asher*

Department of Chemistry, University of Pittsburgh, Pittsburgh, Pennsylvania 15260, United States

Supporting Information

ABSTRACT: We utilize 198 and 204 nm excited UV resonance Raman spectroscopy (UVRR) and circular dichroism spectroscopy (CD) to monitor the backbone conformation and the Gln side chain hydrogen bonding (HB) of a short, mainly polyGln peptide with a $D_2Q_{10}K_2$ sequence (Q10). We measured the UVRR spectra of valeramide to determine the dependence of the primary amide vibrations on amide HB. We observe that a nondisaggregated Q10 (NDQ10) solution (prepared by directly dissolving the original synthesized peptide in pure water) exists in a β-sheet conformation, where the Gln side chains form hydrogen bonds to either the backbone or other Gln side chains. At 60 °C, these solutions readily form amyloid fibrils. We used the polyGln disaggregation protocol of Wetzel et al. [Wetzel, R., et al. (2006) *Methods Enzymol. 413*, 34−74] to dissolve the Q10 β-sheet aggregates. We observe that the disaggregated Q10 (DQ10) solutions adopt PPII-like and 2.5_1-helix conformations where the Gln side chains form hydrogen bonds with water. In contrast, these samples do not form fibrils. The NDQ10 β-sheet solution structure is essentially identical to that found in the NDQ10 solid formed upon evaporation of the solution. The DQ10 PPII and 2.5_1-helix solution structure is essentially identical to that in the DQ10 solid. Although the NDQ10 solution readily forms fibrils when heated, the DQ10 solution does not form fibrils unless seeded with the NDQ10 solution. This result demonstrates very high activation barriers between these solution conformations. The NDQ10 fibril secondary structure is essentially identical to that of the NDQ10 solution, except that the NDQ10 fibril backbone conformational distribution is narrower than in the dissolved species. The NDQ10 fibril Gln side chain geometry is more constrained than when NDQ10 is in solution. The NDQ10 fibril structure is identical to that of the DQ10 fibril seeded by the NDQ10 solution.

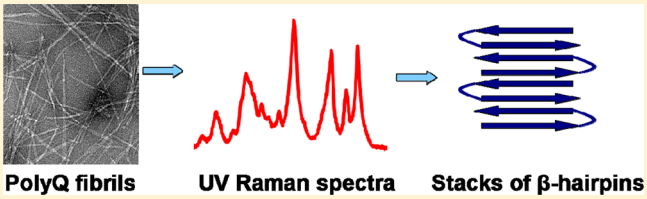

There are at least nine neurodegenerative diseases that are caused by long CAG DNA repeats that encode proteins with long tracts of polyGln residues.[1,2] In these diseases, the extended polyGln regions aggregate to form amyloid fibrils.[3−5] Previous studies suggest that polyGln fibril structures are stabilized by both main chain and side chain hydrogen bonding (HB).[6−9] However, there has been little examination of the role of HB in the aggregation mechanism(s) of polyGln rich peptides and proteins.[10]

Given the central role that backbone and side chain HB can potentially play in stabilizing polyGln aggregates, it is important to find spectral markers for tracking these hydrogen bonds. Backbone HB is sometimes monitored by measuring the frequencies of the backbone amide vibrations, such as the AmI vibration (mainly C═O s) and the AmIII vibration (mainly in-phase combination of CN s and NH b) and the N−H stretching vibration.[11−16] The frequency of the AmII vibration (mainly out-of-phase combination of CN s and NH b) also depends on backbone HB.[17]

However, a method for studying side chain HB is needed. The C═O stretching frequencies of Asn, Gln, protonated Asp, and Glu side chains are sensitive to HB.[18−20] Unfortunately, the use of IR spectroscopy for monitoring side chain vibrations is challenging because of spectral congestion, and isotopic labeling is often required to unambiguously assign bands. Solid state NMR spectroscopy (ssNMR) has been used to characterize Gln side chain HB.[21,22] However, ssNMR requires long measurement times and often requires sophisticated isotope labeling.

In this work, we show that UVRR can selectively enhance the Gln primary amide side chain vibrations, and that these vibrations can be used to track Gln side chain HB. Here, we utilize 198 and 204 nm excited UVRR and CD to monitor the backbone conformation and the Gln side chain HB of a short, mainly polyGln peptide Q10, with a $D_2Q_{10}K_2$ sequence. Previous studies of similar peptides have shown that these peptides can aggregate to form β-sheet rich amyloid fibrils.[8,9,23−29] We observe that nondisaggregated Q10 (NDQ10) in solution occurs as β-sheets in which the Gln side chains form hydrogen bonds to either the backbone or other Gln side chains. At 60 °C, these solutions readily form amyloid fibrils. We used the polyGln disaggregation protocol of Wetzel et al.[30] to disaggregate Q10. We observe that a disaggregated Q10 (DQ10) solution adopts PPII-like and 2.5_1-helix conformations in which the Gln side chains form hydrogen bonds to water. These samples do not form fibrils. Addition of small quantities of NDQ10 solution readily

Received: April 30, 2012
Revised: June 28, 2012
Published: July 2, 2012

dx.doi.org/10.1021/bi300551b | *Biochemistry* 2012, 51, 5822−5830

nucleates fibrils. This directly demonstrates that a high activation barrier exists between the monomer extended DQ10 solution conformation and the β-sheet structures that fibrillize.

EXPERIMENTAL PROCEDURES

Materials. The short mainly polyGln peptide with a $D_2Q_{10}K_2$ sequence (Q10) (>90% pure) was synthesized by AnaSpec Inc. by using a solid-phase peptide synthesis method. Briefly, the first amino acid Fmoc-AA-OH was coupled to the resin, and the peptide was synthesized through sequential synthetic operations of Fmoc deprotection, washing, Fmoc amino acid coupling, and washing. The synthesized crude peptide was obtained after acid cleavage from the solid support resin using a trifluoroacetic acid (TFA) cocktail (where TFA is the major component).

The resulting crude peptide was then purified via preparative high-performance liquid chromatography (using large columns and high flow rates) by using a mobile-phase gradient consisting of 0.1% (v/v) TFA in water and pure acetonitrile. The purified sample was then lyophilized.

Valeramide (97% pure) was purchased from Alfa Aesar. L-Glutamine (99% pure) was purchased from Acros. TFA (99.5% pure) was purchased from Acros. 1,1,1,3,3,3-Hexafluoro-2-propanol (HFIP, ≥99% pure) was purchased from Fluka.

Solutions of nondisaggregated Q10 (NDQ10) were prepared by directly dissolving the peptide in pure water at a concentration of 1 mg/mL at pH 4.3. NDQ10 solid samples were prepared by evaporating the NDQ10 solution. The UVRR spectra were identical to that of the solid sample obtained from the manufacturer. We used the polyGln disaggregation protocol of Wetzel et al.[30] to dissolve the Q10 aggregates. Briefly, solutions of disaggregated Q10 (DQ10) were prepared by suspending 10 mg of Q10 in a 5 mL solution of a 1:1 (v/v) TFA/HFIP mixture [TFA alone dissolves Q10 aggregates (see Figure S3 of the Supporting Information); the primary function of HFIP is to facilitate the removal of TFA[30]]. The samples were then sonicated for 20 min [sonication is not essential (see Figure S3 of the Supporting Information)] and incubated at room temperature for ~2 h. The solvents were evaporated with a gentle stream of dry N_2 gas for ~20 min. The peptide film was resuspended in pure water at a final concentration of ~1 mg/mL, and the pH was adjusted to 7. The peptide solution was centrifuged at 627000*g* for 30 min at 4 °C, and the top 66% of the solution was used. DQ10 solid samples were prepared by evaporating the DQ10 solution. NDQ10 fibrils were prepared by incubating a 4 mg/mL NDQ10 solution at 60 °C for ~1 week (60 °C was chosen to accelerate the reaction). DQ10 fibrils were prepared by incubating a 4 mg/mL DQ10 solution after seeding with a 2% NDQ10 solution at 60 °C for ~4 days. Fibrils were harvested by centrifugation at 627000*g* for 15 min.

CD spectra between 190 and 250 nm were measured by using a Jasco-715 spectropolarimeter with a 0.02 cm path length cuvette. Five 1 min accumulations were averaged.

The UVRR spectrometer was described in detail by Bykov et al.[31] Briefly, 204 nm UV light was obtained by generating the fifth anti-Stokes Raman harmonic of the third harmonic of a Nd:YAG laser (Coherent, Infinity); 198 nm UV light was obtained by mixing the third harmonic of 792 nm light with the fundamental of a 1 kHz repetition rate tunable Ti:sapphire laser (DM20-527 TU-L-FHG) from Photonics Industries.

The liquid sample was circulated in a free surface, temperature-controlled stream. A spinning cell was used for the solid samples to minimize photodegradation; the solid samples were packed into a circular groove of the cylindrical spinning disk. The fibrils were resuspended in 100 μL of pure water and transferred into a spinning Suprasil NMR tube. A 165° sampling backscattering geometry was used. The collected light was dispersed by a double monochromator onto a back-thinned CCD camera with a Lumogen E coating (Princeton Instruments, Spec 10 System). We averaged four 5 min accumulations. The Raman spectral frequencies are accurate to ±1 cm^{-1}. The relative standard deviations in spectral intensities are ≤1%.

Electron micrographs were measured by using a Tecnai T12 microscope (FEI) operating at 120 kV. Samples were prepared on carbon-coated grids and stained with 2% uranyl acetate. Samples were magnified 30000×.

X-ray patterns were measured by using a Bruker Smart Apex CCD diffractometer.

RESULTS

UVRR of Valeramide. We examined the UVRR spectra of valeramide to model the Gln side chain primary amide UVRR spectra, to determine the dependence of the primary amide vibrations on their HB to water. Excitation at both 198 and 204 nm occurs within the $\pi \rightarrow \pi^*$ electronic transition of the primary amide group.[32] Thus, the side chain amide group vibrations are selectively enhanced.

Figure 1 shows the 204 nm excited UVRR spectra of valeramide in water at 22 and 65 °C. The 22 °C spectrum

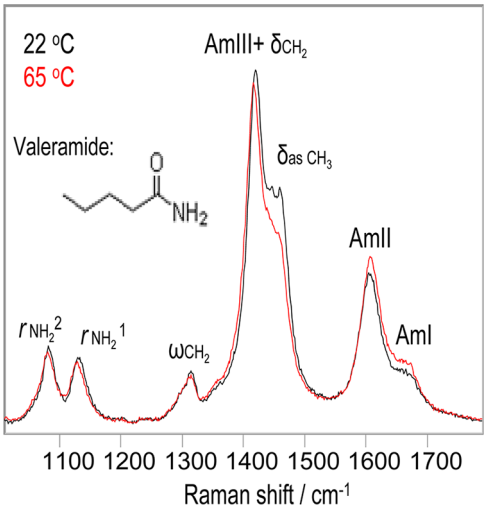

Figure 1. Temperature dependence of the 204 nm excited UVRR spectra of valeramide in water at 22 (black) and 65 °C (red). Water contributions were removed. The intensities were normalized to the 932 cm^{-1} ClO_4^- peak height.

shows an AmI-like shoulder at ~1666 cm^{-1} (mainly CO s) and an AmII-like band at 1606 cm^{-1} (mainly NH_2 b with a small contribution from CO s). It also shows a δ_{asCH_3} shoulder at 1458 cm^{-1} (asymmetric deformation of the CH_3 group) and a strong peak at 1420 cm^{-1} where the δ_{CH_2} band (CH_2 b) and an AmIII-like band (mainly CN s with minor contributions from CH_2 b and NH_2 r) overlap. The ω_{CH_2} band occurs at 1312 cm^{-1} (CH_2 w). The $r_{NH_2}{}^1$ and $r_{NH_2}{}^2$ bands (mainly NH_2 r) occur at 1132 and 1082 cm^{-1}, respectively.[32−34]

dx.doi.org/10.1021/bi300551b | *Biochemistry* 2012, 51, 5822−5830

As the temperature increases to 65 °C, the AmI band frequency changes little. The AmII band upshifts 2 cm^{-1}. The δ_{asCH_3} band downshifts 2 cm^{-1}, and its intensity decreases. The AmIII+δ_{CH_2} peak downshifts 4 cm^{-1}. The ω_{CH_2} band does not change. The $r_{NH_2}{}^1$ and $r_{NH_2}{}^2$ bands both downshift 2 cm^{-1}.

In Acetonitrile. The UVRR spectrum of valeramide in pure acetonitrile (Figure 2) changes dramatically compared to that in pure water. The AmI band upshifts 21 cm^{-1} because of the weakened HB of the carbonyls in acetonitrile,[17] and its relative intensity dramatically increases. The AmII band upshifts 11 cm^{-1} because of the weakened HB of the NH_2 group. The frequency of the δ_{asCH_3} band shows little change. The AmIII +δ_{CH_2} peak and ω_{CH_2} bands downshift 31 and 12 cm^{-1}, respectively. The $r_{NH_2}{}^1$ and $r_{NH_2}{}^2$ bands downshift 6 and 16 cm^{-1}, respectively.

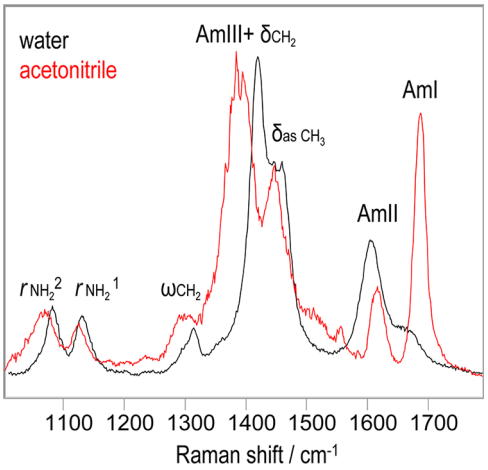

Figure 2. UVRR spectra of valeramide excited at 204 nm and 22 °C: in water (black) and in pure acetonitrile (red). Solvent contributions were removed. The intensities were normalized to the AmIII+δ_{CH_2} peak height.

Solid State. The UVRR spectrum of valeramide powder from the manufacturer (Figure 3, red) differs significantly from that dissolved in water. The AmI band upshifts 10 cm^{-1}, indicative of weakened carbonyl HB,[17] and the relative intensity of the AmI band significantly increases. The AmII band downshifts 5 cm^{-1}. The AmIII+δ_{CH_2} peak becomes asymmetric and upshifts 12 cm^{-1}. The δ_{asCH_3} band is not evident. The frequency of the ω_{CH_2} band changes little. The $r_{NH_2}{}^1$ and $r_{NH_2}{}^2$ bands upshift 10 and 8 cm^{-1}, respectively.

Raman Cross Sections for Valeramide. We calculated the Raman cross sections for valeramide in water and in acetontrile by using eq 1:[35]

$$\sigma_{val} = \frac{I_{val}k(\lambda_r)C_r\sigma_r}{I_r k(\lambda_{val})C_{val}}\left(\frac{\varepsilon_{val}+\varepsilon_{ex}}{\varepsilon_r+\varepsilon_{ex}}\right) \quad (1)$$

where I_{val} and I_r are the relative intensities of the valeramide band and the internal standard band (which is the 932 cm^{-1} ClO_4^- band in aqueous solution or the 918 cm^{-1} C−C stretching band of acetonitrile in pure acetonitrile[36]). $k(\lambda_r)$ and $k(\lambda_{val})$ are the spectrometer efficiencies at the wavelengths of the internal standard and valeramide Raman bands, respectively. C_r and C_{val} are the concentrations of the internal standard and valeramide, respectively. σ_r is the total differential Raman cross section of the internal standard band at the excitation frequency, ν_{ex}. ε_{ex} is the sample molar absorptivity at ν_{ex}. ε_{val} and ε_r are the sample molar absorptivities at the valeramide Raman band frequency and the internal standard band frequency, respectively. The expression in the parentheses approximately corrects the Raman intensities for self-absorption in a backscattering geometry.

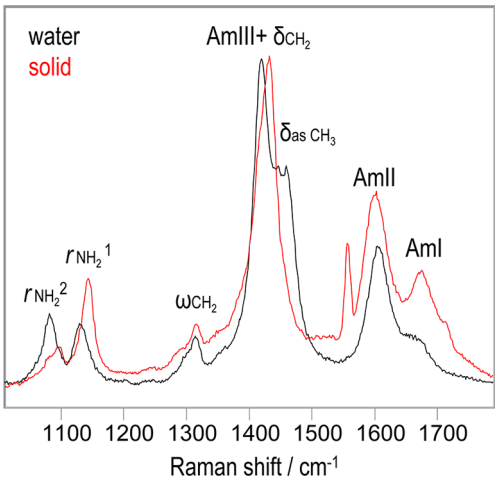

Figure 3. UVRR spectra of valeramide excited at 204 nm in solid form (red) and in water (black) at 22 °C. Water contributions were removed. The intensities were normalized to the AmIII+δ_{CH_2} peak height.

Table 1 shows the measured total differential Raman cross sections for valeramide. The 204 nm Raman cross section values of the valeramide amide bands in pure water are approximately half of those of protein backbone secondary amide bands,[37] presumably because the primary amide group electronic transition is blue-shifted from that of the peptide bond secondary amides.[32]

The Raman cross sections of the valeramide bands in pure acetonitrile are smaller than those in pure water, except for the AmI band cross section, which is doubled. A similar behavior was observed for the AmI band of *N*-methylacetamide.[38] The increased cross section was ascribed to a larger relative CO bond excited state displacement in acetonitrile.[38] The Raman cross sections of the valeramide bands generally triple as the excitation wavelength decreases from 204 to 198 nm, except for the AmII band cross section in acetonitrile, which increases by >10-fold. The 198 nm Raman cross section values of the valeramide primary amide bands are similar to those of the protein backbone secondary amide bands.[37]

Effects of Hydrogen Bonding on the Frequencies of Primary Amide Vibrations. These UVRR studies of valeramide indicate that the AmI, AmII, $r_{NH_2}{}^1$, and $r_{NH_2}{}^2$ frequencies of the primary amide depend on HB. Water HB to the carbonyls downshifts the AmI band by 21 cm^{-1} (see Table 2), while HB to the NH_2 group upshifts the $r_{NH_2}{}^1$ and $r_{NH_2}{}^2$ bands by 6 and 16 cm^{-1}, respectively; the AmII band downshifts 11 cm^{-1} upon the formation of hydrogen bonds to the NH_2 group. The solid state AmI band upshifts 10 cm^{-1} relative to that in water, indicating weaker carbonyl HB in the valeramide solid than in water. The solid state AmII band downshifts 7 cm^{-1} compared to that in water, and the $r_{NH_2}{}^1$ and

dx.doi.org/10.1021/bi300551b | *Biochemistry* 2012, 51, 5822−5830

Table 1. Measured Total Differential Raman Cross Sections for Valeramide (mbarn molecule^{-1} sr $^{-1}$) at 22 °C[a]

		AmI	AmII	δ_{asCH_3}	AmIII+δ_{CH_2}	ω_{CH_2}	$r_{NH_2}{}^1$	$r_{NH_2}{}^2$
ν_{ex} = 204 nm	in water	5.4	17	21	33	3.3	5.0	5.6
	in acetonitrile	11	3.1	13	29	3.2	1.7	4.4
ν_{ex} = 198 nm	in water	14	52	58	94	11	14	15
	in acetonitrile	41	50	35	91	10	12	16

[a]We did not calculate the Raman cross sections for valeramide powder because of the lack of an intensity internal standard.

Table 2. Measured AmI, AmII, $r_{NH_2}{}^1$, and $r_{NH_2}{}^2$ Frequencies of Valeramide

	AmI (cm^{-1})	AmII (cm^{-1})	$r_{NH_2}{}^1$ (cm^{-1})	$r_{NH_2}{}^2$ (cm^{-1})
in water at 22 °C	1666	1606	1132	1082
in water at 65 °C	1666	1608	1130	1080
in acetonitrile at 22 °C	1687	1617	1126	1066
solid at 22 °C	1676	1601	1142	1090

$r_{NH_2}{}^2$ bands upshift 12 and 10 cm^{-1}, respectively. This indicates stronger NH_2 group HB in the valeramide solid than in water.

X-ray studies of butyramide solid[39] (which has one fewer methylene than valeramide) indicate that each carbonyl forms two hydrogen bonds to the two amine H atoms of two adjacent molecules, while each NH_2 group forms two hydrogen bonds to two carbonyls. This stronger NH_2 group HB may result from the fact that while the valeramide carbonyl HB geometry is more optimized in water than in the solid state, the NH_2 group HB is stronger in the solid state.

Q10 Solution Backbone Conformation. We performed both CD and UVRR measurements to examine the Q10 solution backbone conformation. Previous studies of similar peptides indicate that nondisaggregated polyGln peptides in aqueous solutions occur as β-sheets,[24] while freshly disaggregated polyGln peptides adopt extended conformations.[40,41]

Figure 4 shows the CD spectra of Q10 solutions. The CD spectrum of the NDQ10 in pure water (---) shows a trough at

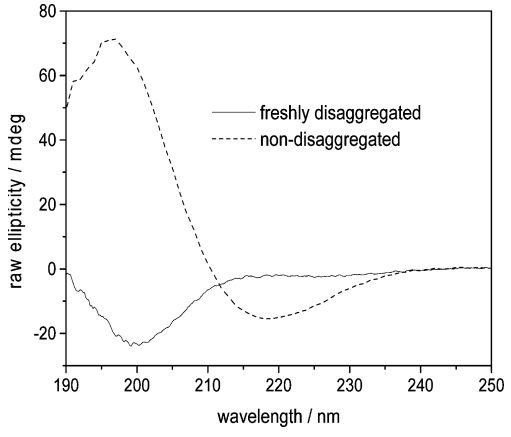

Figure 4. CD spectra of 1 mg/mL DQ10 (—) and NDQ10 (---) in pure water at 22 °C. Measured by using a 0.02 cm path length cuvette.

~218 nm and a strong positive band at 197 nm, both characteristic of β-sheets.[42] The spectrum of DQ10 in pure water (—) shows a very slight negative ellipticity at ~220 nm and a strong negative band at 200 nm, indicative of extended conformations.[43−45]

Excitation at 204 nm occurs within the $\pi \rightarrow \pi^*$ electronic transition of the backbone secondary amides[37] and to the long wavelength side of the side chain primary amide electronic transitions.[32] Figure 5 shows that the 204 nm excited UVRR

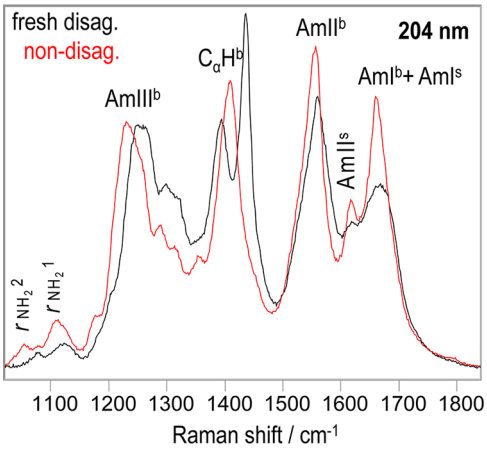

Figure 5. UVRR spectra of DQ10 (black) and NDQ10 (red) excited at 204 nm in pure water at 22 °C. A superscript b indicates a backbone vibration; a superscript s indicates a side chain vibration. The intensities were normalized to the AmIII^b peak height.

spectra of Q10 solutions are dominated by the backbone amide vibrations (indicated by a superscript b). The backbone amide vibrations are more enhanced by 204 nm excitation than are those of the side chain amides (indicated by a superscript s; the side chain amide bands were assigned on the basis of the measured valeramide primary amide band frequencies).[32]

The UVRR spectrum of NDQ10 (red) shows an AmI^b band at ~1660 cm^{-1}, an AmII^b band at ~1550 cm^{-1}, the (C)C$_\alpha$−H^b bending bands at ~1400 cm^{-1}, and the AmIII^b region between 1180 and 1330 cm^{-1}. The AmI^b band overlaps with the Gln side chain AmI^s band; the C$_\alpha$H^b bending band overlaps with the side chain AmIII^s+δ_{CH_2} peak.

The AmIII^b region of Q10 contains no overlapping side chain contributions. We calculated the Ramachandran Ψ probability distributions for the Q10 backbone peptide bonds from the UVRR spectra of Figure 5 by using the methodology of Mikhonin et al.[11,46,47] This method correlates different AmIII$_3$ frequencies of the band envelope to different peptide bond Ψ angles. This deconvolutes the inhomogeneously broadened AmIII band shape to a Ψ angle distribution (see the Supporting Information for details). The estimated error of this Ramachandran Ψ angle determination was suggested to be no more than ±14°.[11]

The Ψ distribution in Figure 6 for NDQ10 shows a dominant β-sheet contribution (Ψ ~ 138°). It also contains contributions from type I, type III, or type VIII β-turn regions (Ψ ~ −40°). The Ψ distribution for DQ10 shows a dominant contribution of PPII-like (Ψ ~ 145°) and 2.5$_1$-helix

dx.doi.org/10.1021/bi300551b | Biochemistry 2012, 51, 5822−5830

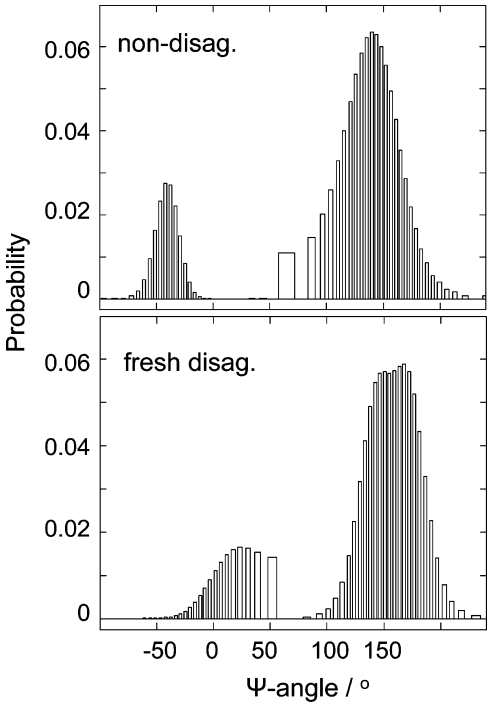

Figure 6. Calculated Ψ angle distributions for NDQ10 and DQ10 in pure water at 22 °C.

conformations (Ψ ~ 170°). It also contains contributions of type I′ or type III′ β-turns (Ψ ~ 30°).

Previous studies indicate that poly-L-lysine and poly-L-glutamate adopt 2.5_1-helix conformations that are stabilized by electrostatic repulsion between the charged side chains.[48−50] We surprisingly find that DQ10 adopts 2.5_1-helix conformations. The mechanism(s) by which these 2.5_1-helix conformations of Q10 are stabilized is unknown.

Q10 Solution Side Chain Hydrogen Bonding. Excitation at 198 nm (Figure 7) enhances the primary amide UVRR bands significantly more than does 204 nm excitation. As a result, the difference spectrum between the 198 and 204 nm excited UVRR spectra of Q10 (Figure 7) is dominated by the Gln side chain primary amide bands.

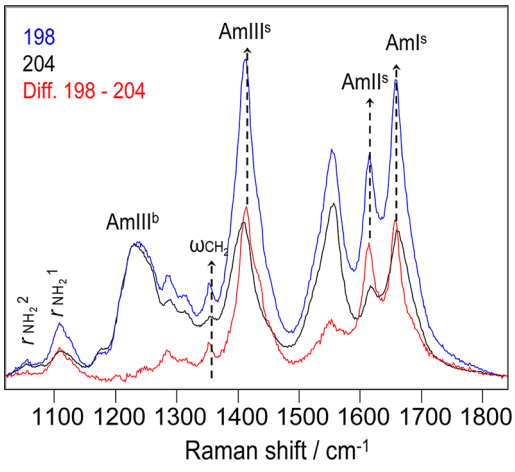

Figure 7. UVRR spectra of NDQ10 excited at 198 (blue) and 204 nm (black) in pure water at 22 °C and the difference spectrum between them (red). The intensities were normalized to the AmIII^b peak height before spectral subtraction.

The 198 minus 204 nm difference spectrum of NDQ10 in pure water (Figure 8) shows an AmI^s band at 1657 cm^{-1} and an

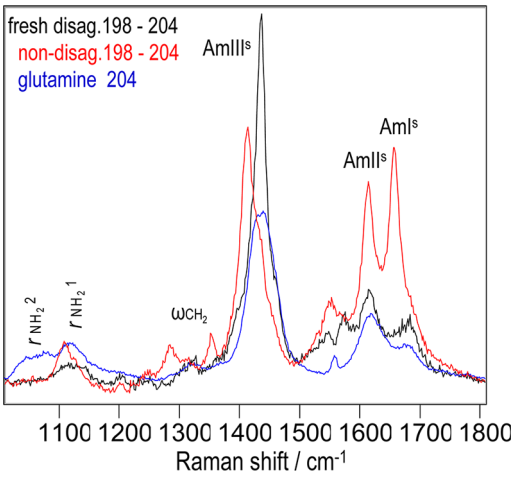

Figure 8. Difference spectra between the 198 and 204 nm excited UVRR spectra of NDQ10 (red) and DQ10 (black) in pure water at 22 °C. UVRR spectrum of glutamine excited at 204 nm in pure water at pH 1.6 and 22 °C (blue).

AmII^s band at 1614 cm^{-1}. It also shows an AmIII^s band at 1414 cm^{-1} and an ω_{CH_2} band at 1353 cm^{-1}. The $r_{NH_2}{}^1$ and $r_{NH_2}{}^2$ bands occur at 1110 and 1056 cm^{-1}, respectively.

The 198 minus 204 nm difference spectrum of DQ10 in pure water (Figure 8, black) differs significantly from that of NDQ10. The DQ10 AmI^s band upshifts 26 cm^{-1}, indicating weaker HB of the Gln side chain carbonyls than in NDQ10. The AmII^s frequency shows little change. The AmIII^s frequency upshifts 22 cm^{-1}. The DQ10 $r_{NH_2}{}^1$ and $r_{NH_2}{}^2$ frequencies upshift 13 and 19 cm^{-1}, respectively, indicating stronger HB of the Gln side chain NH_2 group than in NDQ10.

The frequencies of the Gln primary amide vibrations of DQ10 in pure water (Figure 8, black) are very similar to those of glutamine in pure water (Figure 8, blue); the UVRR spectrum of glutamine excited at 204 nm contains only side chain amide vibrations, and there are no secondary amides. This indicates that HB of the Gln side chains of DQ10 is similar to that of glutamine in pure water; i.e., the Gln side chains of DQ10 form hydrogen bonds to water.

The DQ10 AmIII^s band is significantly narrower than that of glutamine in water. This may result from the fact that the glutamine side chain has conformations in solution where the primary amide side chain interacts with the NH_3^+ groups.

Previous studies indicated that polyGln aggregates adopt β-sheet conformations that are stabilized by both main chain and side chain HB.[6−9] We observe that the Gln side chain HB of NDQ10 differs significantly from that of DQ10. The NDQ10 AmI^s frequency downshifts 26 cm^{-1} relative to that of DQ10, and its $r_{NH_2}{}^1$ and $r_{NH_2}{}^2$ frequencies downshift 13 and 19 cm^{-1}, respectively. Table 2 shows that HB to the primary amide carbonyls significantly downshifts the AmI^s frequency, while HB to the NH_2 group upshifts the $r_{NH_2}{}^1$ and $r_{NH_2}{}^2$ frequencies. Thus, the HB of the NDQ10 Gln side chain carbonyls is stronger than that of DQ10, while the HB of NDQ10 Gln side chain NH_2 groups are weaker than that of DQ10. These results indicate that the Gln side chain carbonyls of NDQ10 do not form hydrogen bonds to water. Instead, they form hydrogen

dx.doi.org/10.1021/bi300551b | *Biochemistry* 2012, 51, 5822−5830

bonds to the backbone NH group or to Gln side chain NH_2 group. Presumably, this conformation results in weaker NH_2 group HB.

Q10 Solids. We measured the UVRR spectra of Q10 solids excited at 204 nm formed by evaporation of the NDQ10 and DQ10 solutions. The UVRR spectral frequencies of the NDQ10 solid (Figure 9, black) are very similar to those of

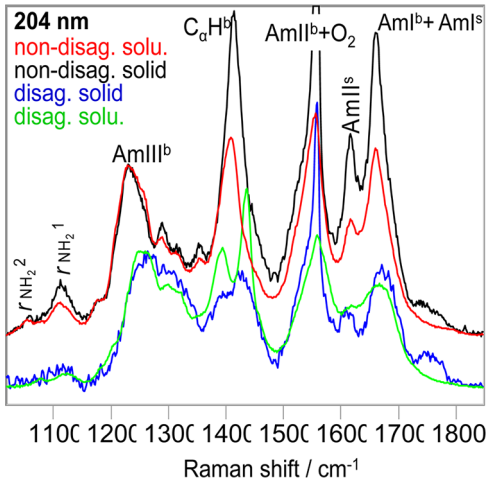

Figure 9. UVRR spectra of the NDQ10 solid (black) and solution (red) and the DQ10 solid (blue) and solution (green) excited at 204 nm at 22 °C. A superscript b indicates backbone vibration; a superscript s indicates side chain vibration. The intensities were normalized to the $AmIII^b$ peak height.

NDQ10 in solution (Figure 9, red), indicating that the backbone conformations and the Gln side chain HB of the NDQ10 solid and solution are essentially identical, and mainly β-sheet. The NDQ10 solid shows a powder X-ray pattern (Figure 10) very similar to that of Perutz et al.[23] The 4.75 Å reflection (Figure 10) is characteristic of β-sheet structures.[23]

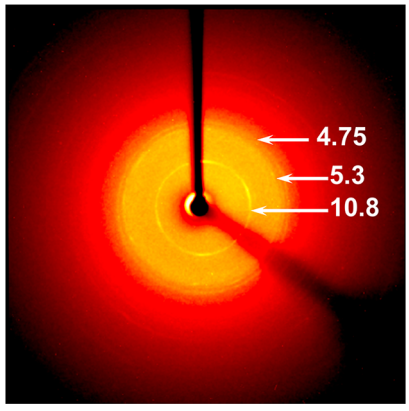

Figure 10. Powder X-ray diffraction of the NDQ10 solid. The sample was prepared by slowly evaporating the NDQ10 solution on a glass slide over ~2 days.

The $AmIII^b$ region of the solvent-evaporated DQ10 solid (Figure 9, blue) is similar to that of the DQ10 solution (Figure 9, green), indicating that their Q10 backbone conformations are similar. The solid state $AmII^b$ band downshifts 7 cm^{-1} compared to that of solution, indicating weakened HB of the solid state backbone NH group,[17] while the solid state AmI^b and AmI^s bands upshift 5 cm^{-1} relative to that of the solution, indicating weakened HB to the solid backbone carbonyls and the Gln side chain carbonyls.[17]

These results indicate the Q10 solution and solid state conformations are essentially identical. This suggests that the solution state activation barriers between extended PPII and 2.5_1-helix conformations and the β-sheet aggregate conformations are very high; these structures are not in equilibrium in solution or during evaporation of the solution.

Fibrillization of the Q10 Solution. We observe that NDQ10 in pure water forms amyloid fibrils after incubation at 60 °C for ~2 days [confirmed by using TEM and the ThT binding assay;[24] the short time TEM of NDQ10 does not show fibril structures (see Figure S4 of the Supporting Information)]. In contrast, DQ10 does not form fibrils even after incubation for >2 weeks at 60 °C. However, upon being seeded with a small aliquot of the NDQ10 solution, the DQ10 solution readily forms fibrils at 60 °C (confirmed by using TEM and the ThT binding assay). Thus, NDQ10 appears to contain small aggregates that seed fibrillization.

Thus, the activation barrier for DQ10 to form β-sheet aggregates that evolve to NDQ10 fibrils is quite high. The fact that DQ10 solutions do not self-nucleate fibrils is consistent with previous studies of similar peptides.[24,51,52]

Q10 Fibrils. Panels a and b of Figure 11 show electron micrographs of the NDQ10 fibrils and the DQ10 fibrils formed upon seeding with the NDQ10 solution, respectively. Figure 11c shows the 204 nm excited UVRR spectra of the NDQ10 fibrils, the DQ10 fibrils and the UVRR spectrum of the NDQ10 solution.

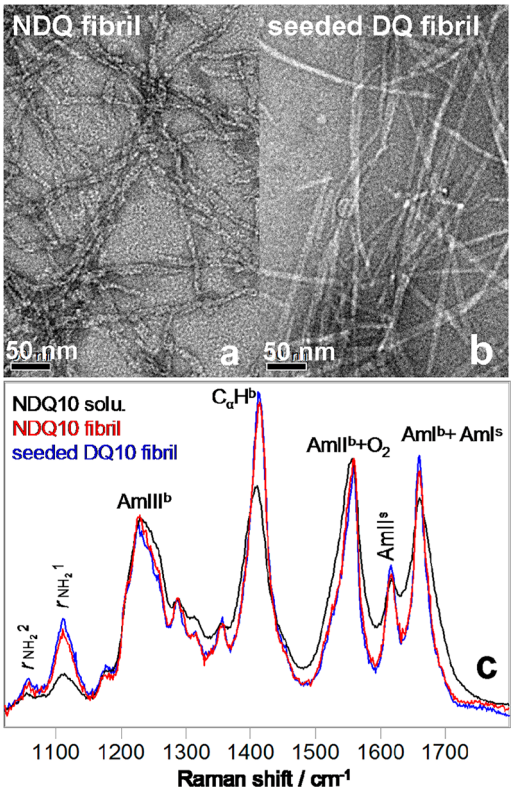

Figure 11. Electron micrographs of (a) NDQ10 fibrils in pure water after incubation at 60 °C for ~1 week and (b) DQ10 fibrils in pure water upon being seeded with a 2% NDQ10 solution after incubation at 60 °C for ~4 days. (c) UVRR spectra of the NDQ10 fibrils, the DQ10 fibrils, and the NDQ10 solution excited at 204 nm at 22 °C.

dx.doi.org/10.1021/bi300551b | Biochemistry 2012, 51, 5822−5830

The NDQ10 fibril band frequencies (Figure 11c, red) are very similar to those of the NDQ10 solution (Figure 11c, black). Thus, the NDQ10 fibrils also occur in a β-sheet structure in which the Gln side chains form hydrogen bonds to the backbone or to other Gln side chains. However, the NDQ10 fibril bands are significantly narrowed compared to those in the NDQ10 solution, indicating a narrower backbone conformational distribution and more constrained Gln side chain geometries for the NDQ10 fibrils than for the NDQ10 solution.

The UVRR spectrum of the DQ10 fibrils formed upon seeding with an aliquot of the NDQ10 solution (Figure 11c, blue) is identical to that of the NDQ10 fibrils spontaneously formed (Figure 11c, red), indicating identical Q10 backbone conformations and Gln side chain HB.

DISCUSSION

Q10 Structure. CD and UVRR studies indicate that NDQ10 in pure water adopts a predominantly β-sheet structure, consistent with previous studies indicating that polyGln aggregates form β-sheet rich structures[24,53] UVRR also reveals turn conformations in NDQ10. The fractions of β-sheet and turn conformations are 0.84 and 0.16, respectively. This ratio suggests that NDQ10 in pure water occurs as β-hairpins in which 2 residues are in the turn region and 11 residues form a β-sheet structure (Figure 12).

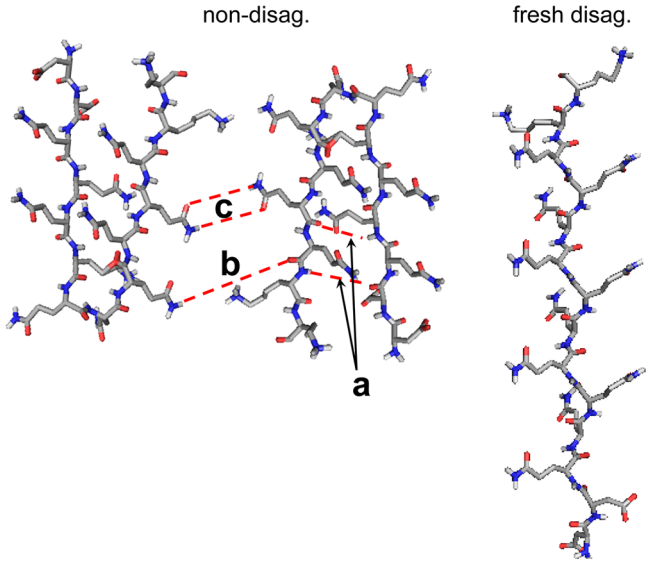

Figure 12. Proposed structures of NDQ10 and DQ10. NDQ10 occurs as β-sheets in which the Gln side chains form hydrogen bonds to the backbone or other Gln side chains. DQ10 adopts PPII and 2.5_1-helix conformations in which the Gln side chains form hydrogen bonds to water: main chain−main chain HB (a), main chain−side chain HB (b), and side chain−side chain HB (c).

We observe that DQ10 in pure water adopts predominantly PPII-like and 2.5_1-helix conformations (Figure 12). Previous studies indicate that glutamine residues in short polyGln sequences have a strong propensity to form PPII-like conformations;[40,41] other studies, however, report disordered structures.[29,51,54−57]

UVRR indicates that the Gln side chains of NDQ10 form hydrogen bonds to the backbone or other Gln side chains, while the Gln side chains of DQ10 form hydrogen bonds to water.

We also observe that the NDQ10 fibril secondary structure is essentially identical to that in the NDQ10 solution, except that the NDQ10 fibril backbone conformational distribution is narrower. Also, the fibril Gln side chain geometry is more constrained than that of the NDQ10 solution.

The UVRR-determined NDQ10 fibril structure appears to be identical to that of the DQ10 fibrils seeded by an aliquot of the NDQ10 solution. These results suggest that the Q10 fibrils consist of stacks of β-hairpins. Previous studies of a similar peptide with a $D_2Q_{15}K_2$ sequence also indicated β-hairpin fibril structure.[8,9,25]

CONCLUSIONS

We utilized UVRR and CD to monitor the backbone conformation and the Gln side chain HB of a short mainly polyGln peptide Q10, with a $D_2Q_{10}K_2$ sequence. We measured UVRR spectra of valeramide to determine the dependence of primary amide vibrations on the primary amide hydrogen bonding. We observe that NDQ10 occurs in a β-sheet-like structure in which the Gln side chains form hydrogen bonds to the backbone or other Gln side chains.

These NDQ10 solutions readily form amyloid fibrils. In contrast, DQ10 solutions adopt PPII-like and 2.5_1-helix conformations in which the Gln side chains form hydrogen bonds to water. These samples do not form fibrils upon being heated within 2 weeks. The NDQ10 and DQ10 solution structures are essentially identical to their solid state structures. Although the NDQ10 solution readily forms fibrils when heated, the DQ10 solution does not form fibrils unless seeded by the NDQ10 solution. This indicates very high activation barriers occur between these solution conformations.

The Q10 fibril secondary structure is essentially identical to that of the NDQ10 solution, except that the fibril backbone conformational distribution is narrower and its Gln side chain geometry is more constrained compared to that of the NDQ10 solution.

ASSOCIATED CONTENT

Supporting Information

Methods for the determination of Ψ angle distributions from UVRR spectra and CD spectra of Q10 solutions in different solvents for disaggregation. This material is available free of charge via the Internet at http://pubs.acs.org.

AUTHOR INFORMATION

Corresponding Author

*E-mail: asher@pitt.edu. Phone: (412) 624-8570.

Present Address

[†]Department of Chemistry, Northwestern University, Evanston, IL 60208.

Funding

This work was supported by National Institutes of Health Grant 1RO1EB009089.

Notes

The authors declare no competing financial interest.

ACKNOWLEDGMENTS

We thank Dr. Sergei V. Bykov for useful discussions. We also thank Dr. Lu Ma for help with instrumentation.

REFERENCES

(1) Zoghbi, H. Y., and Cummings, C. J. (2000) Fourteen and counting: Unraveling trinucleotide repeat diseases. *Hum. Mol. Genet. 9*, 909−916.

(2) Ross, C. A., and Poirier, M. A. (2005) What is the role of protein aggregation in neurodegeneration? *Nat. Rev. Mol. Cell Biol. 6*, 891−898.

(3) Wetzel, R., Bhattacharyya, A. M., and Thakur, A. K. (2005) Polyglutamine aggregation nucleation: Thermodynamics of a highly unfavorable protein folding reaction. *Proc. Natl. Acad. Sci. U.S.A. 102*, 15400−15405.

(4) Wetzel, R., Chen, S. M., and Ferrone, F. A. (2002) Huntington's disease age-of-onset linked to polyglutamine aggregation nucleation. *Proc. Natl. Acad. Sci. U.S.A. 99*, 11884−11889.

(5) Wetzel, R., Slepko, N., Bhattacharyya, A. M., Jackson, G. R., Steffan, J. S., Marsh, J. L., and Thompson, L. M. (2006) Normal-repeat-length polyglutamine peptides accelerate aggregation nucleation and cytotoxicity of expanded polyglutamine proteins. *Proc. Natl. Acad. Sci. U.S.A. 103*, 14367−14372.

(6) Rossetti, G., Magistrato, A., Pastore, A., Persichetti, F., and Carloni, P. (2008) Structural Properties of Polyglutamine Aggregates Investigated via Molecular Dynamics Simulations. *J. Phys. Chem. B 112*, 16843−16850.

(7) Smith, M. H., Miles, T. F., Sheehan, M., Alfieri, K. N., Kokona, B., and Fairman, R. (2010) Polyglutamine fibrils are formed using a simple designed β-hairpin model. *Proteins: Struct., Funct., Bioinf. 78*, 1971−1979.

(8) Perutz, M. F., Johnson, T., Suzuki, M., and Finch, J. T. (1994) Glutamine repeats as polar zippers: Their possible role in inherited neurodegenerative diseases. *Proc. Natl. Acad. Sci. U.S.A. 91*, 5355−5358.

(9) Sikorski, P., and Atkins, E. (2005) New model for crystalline polyglutamine assemblies and their connection with amyloid fibrils. *Biomacromolecules 6*, 425−432.

(10) Nagai, Y., Inui, T., Popiel, H. A., Fujikake, N., Hasegawa, K., Urade, Y., Goto, Y., Naiki, H., and Toda, T. (2007) A toxic monomeric conformer of the polyglutamine protein. *Nat. Struct. Mol. Biol. 14*, 332−340.

(11) Mikhonin, A. V., Bykov, S. V., Myshakina, N. S., and Asher, S. A. (2006) Peptide secondary structure folding reaction coordinate: Correlation between UV Raman amide III frequency, Π Ramachandran angle, and hydrogen bonding. *J. Phys. Chem. B 110*, 1928−1943.

(12) Manas, E. S., Getahun, Z., Wright, W. W., DeGrado, W. F., and Vanderkooi, J. M. (2000) Infrared spectra of amide groups in α-helical proteins: Evidence for hydrogen bonding between helices and water. *J. Am. Chem. Soc. 122*, 9883−9890.

(13) Wang, Y., Purrello, R., Jordan, T., and Spiro, T. G. (1991) UVRR spectroscopy of the peptide bond. 1. Amide S, a nonhelical structure marker, is a CαH bending mode. *J. Am. Chem. Soc. 113*, 6359−6368.

(14) Mirkin, N. G., and Krimm, S. (2004) Structural dependence of NH stretch mode frequency shifts in amide and peptide. *J. Phys. Chem. A 108*, 5438−5448.

(15) Fu, L., Liu, J., and Yan, E. C. Y. (2011) Chiral Sum Frequency Generation Spectroscopy for Characterizing Protein Secondary Structures at Interfaces. *J. Am. Chem. Soc. 133*, 8094−8097.

(16) Fu, L., Wang, Z., and Yan, E. C. (2011) Chiral vibrational structures of proteins at interfaces probed by sum frequency generation spectroscopy. *Int. J. Mol. Sci. 12*, 9404−9425.

(17) Myshakina, N. S., Ahmed, Z., and Asher, S. A. (2008) Dependence of amide vibrations on hydrogen bonding. *J. Phys. Chem. B 112*, 11873−11877.

(18) Barth, A. (2000) The infrared absorption of amino acid side chains. *Prog. Biophys. Mol. Biol. 74*, 141−173.

(19) Takei, K., Takahashi, R., and Noguchi, T. (2008) Correlation between the hydrogen-bond structures and the C═O stretching frequencies of carboxylic acids as studied by density functional theory calculations: Theoretical basis for interpretation of infrared bands of carboxylic groups in proteins. *J. Phys. Chem. B 112*, 6725−6731.

(20) Natalello, A., Frana, A. M., Relini, A., Apicella, A., Invernizzi, G., Casari, C., Gliozzi, A., Doglia, S. M., Tortora, P., and Regonesi, M. E. (2011) A Major Role for Side-Chain Polyglutamine Hydrogen Bonding in Irreversible Ataxin-3 Aggregation. *PLoS One 6*, e18789.

(21) Schneider, R., Schumacher, M. C., Mueller, H., Nand, D., Klaukien, V., Heise, H., Riedel, D., Wolf, G., Behrmann, E., Raunser, S., Seidel, R., Engelhard, M., and Baldus, M. (2011) Structural characterization of polyglutamine fibrils by solid-state NMR spectroscopy. *J. Mol. Biol. 412*, 121−136.

(22) Sivanandam, V. N., Jayaraman, M., Hoop, C. L., Kodali, R., Wetzel, R., and van der Wel, P. C. (2011) The aggregation-enhancing huntingtin N-terminus is helical in amyloid fibrils. *J. Am. Chem. Soc. 133*, 4558−4566.

(23) Perutz, M. F., Finch, J. T., Berriman, J., and Lesk, A. (2002) Amyloid fibers are water-filled nanotubes. *Proc. Natl. Acad. Sci. U.S.A. 99*, 5591−5595.

(24) Chen, S. M., Berthelier, V., Hamilton, J. B., O'Nuallain, B., and Wetzel, R. (2002) Amyloid-like features of polyglutamine aggregates and their assembly kinetics. *Biochemistry 41*, 7391−7399.

(25) Sharma, D., Shinchuk, L. M., Inouye, H., Wetzel, R., and Kirschner, D. A. (2005) Polyglutamine homopolymers having 8−45 residues form slablike β-crystallite assemblies. *Proteins: Struct., Funct., Bioinf. 61*, 398−411.

(26) Lee, C. C., Walters, R. H., and Murphy, R. M. (2007) Reconsidering the mechanism of polyglutamine peptide aggregation. *Biochemistry 46*, 12810−12820.

(27) Darnell, G., Orgel, J. P. R. O., Pahl, R., and Meredith, S. C. (2007) Flanking polyproline sequences inhibit β-sheet structure in polyglutamine segments by inducing PPII-like helix structure. *J. Mol. Biol. 374*, 688−704.

(28) Kar, K., Jayaraman, M., Sahoo, B., Kodali, R., and Wetzel, R. (2011) Critical nucleus size for disease-related polyglutamine aggregation is repeat-length dependent. *Nat. Struct. Mol. Biol. 18*, 328−336.

(29) Walters, R. H., and Murphy, R. M. (2009) Examining Polyglutamine Peptide Length: A Connection between Collapsed Conformations and Increased Aggregation. *J. Mol. Biol. 393*, 978−992.

(30) O'Nuallain, B., Thakur, A. K., Williams, A. D., Bhattacharyya, A. M., Chen, S. M., Thiagarajan, G., and Wetzel, R. (2006) Kinetics and thermodynamics of amyloid assembly using a high-performance liquid chromatography-based sedimentation assay. *Methods Enzymol. 413*, 34−74.

(31) Bykov, S., Lednev, I., Ianoul, A., Mikhonin, A., Munro, C., and Asher, S. A. (2005) Steady-state and transient ultraviolet resonance Raman spectrometer for the 193−270 nm spectral region. *Appl. Spectrosc. 59*, 1541−1552.

(32) Dudik, J. M., Johnson, C. R., and Asher, S. A. (1985) UV Resonance Raman Studies of Acetone, Acetamide, and N-Methylacetamide: Models for the Peptide Bond. *J. Phys. Chem. 89*, 3805−3814.

(33) Kuroda, Y., Saito, Y., Uno, T., and Machida, K. (1972) Vibrational-Spectra of Propionamide and Its C-Deuterated and N-Deuterated Compounds. *Bull. Chem. Soc. Jpn. 45*, 2371−2383.

(34) Nandini, G., and Sathyanarayana, D. N. (2002) Ab initio studies on molecular conformation and vibrational spectra of propionamide. *THEOCHEM 586*, 125−135.

(35) Xiong, K., and Asher, S. A. (2011) Lowest Energy Electronic Transition in Aqueous Cl^- Salts: $Cl^- \rightarrow (H_2O)_6$ Charge Transfer Transition. *J. Phys. Chem. A 115*, 9345−9348.

(36) Dudik, J. M., Johnson, C. R., and Asher, S. A. (1985) Wavelength Dependence of the Preresonance Raman Cross-Sections of CH_3CN, SO_4^{2-}, ClO_4^-, and NO_3^-. *J. Chem. Phys. 82*, 1732−1740.

(37) Sharma, B., Bykov, S. V., and Asher, S. A. (2008) UV resonance Raman investigation of electronic transitions in α-helical and polyproline II-like conformations. *J. Phys. Chem. B 112*, 11762−11769.

(38) Chen, X. G., Asher, S. A., Schweitzerstenner, R., Mirkin, N. G., and Krimm, S. (1995) UV Raman Determination of the $\pi - \pi^*$ Excited-State Geometry of N-Methylacetamide: Vibrational Enhancement Pattern. *J. Am. Chem. Soc. 117*, 2884−2895.

(39) Lewis, T. C., and Tocher, D. A. (2005) A low-temperature determination of butyramide. *Acta Crystallogr. E61*, O1985−O1986.
(40) Chellgren, B. W., Miller, A. F., and Creamer, T. P. (2006) Evidence for polyproline II helical structure in short polyglutamine tracts. *J. Mol. Biol. 361*, 362−371.
(41) Wang, X. L., Vitalis, A., Wyczalkowski, M. A., and Pappu, R. V. (2006) Characterizing the conformational ensemble of monomeric polyglutamine. *Proteins: Struct., Funct., Bioinf. 63*, 297−311.
(42) Woody, R. W. (1996) *Theory of Circular Dichroism of Proteins*, Plenum Press, New York.
(43) Sreerama, N., and Woody, R. W. (1994) Poly(Pro)II Helices in Globular-Proteins: Identification and Circular Dichroic Analysis. *Biochemistry 33*, 10022−10025.
(44) Shi, Z., Olson, C., Rose, G., Baldwin, R., and Kallenbach, N. (2002) Polyproline II structure in a sequence of seven alanine residues. *Proc. Natl. Acad. Sci. U.S.A. 99*, 9190−9195.
(45) Shi, Z., Chen, K., Liu, Z., and Kallenbach, N. (2006) Conformation of the backbone in unfolded proteins. *Chem. Rev. 106*, 1877−1897.
(46) Mikhonin, A. V., and Asher, S. A. (2006) Direct UV Raman monitoring of 3_{10}-helix and π-bulge premelting during α-helix unfolding. *J. Am. Chem. Soc. 128*, 13789−13795.
(47) Asher, S. A., Mikhonin, A. V., and Bykov, S. (2004) UV Raman demonstrates that α-helical polyalanine peptides melt to polyproline II conformations. *J. Am. Chem. Soc. 126*, 8433−8440.
(48) Mikhonin, A. V., Myshakina, N. S., Bykov, S. V., and Asher, S. A. (2005) UV resonance Raman determination of polyproline II, extended 2.5_1-helix, and β-sheet ψ angle energy landscape in poly-L-lysine and poly-L-glutamic acid. *J. Am. Chem. Soc. 127*, 7712−7720.
(49) Ma, L., Ahmed, Z., and Asher, S. A. (2011) Ultraviolet Resonance Raman Study of Side Chain Electrostatic Control of Poly-L-Lysine Conformation. *J. Phys. Chem. B 115*, 4251−4258.
(50) Xiong, K., Ma, L., and Asher, S. A. (2012) Conformation of poly-L-glutamate is independent of ionic strength. *Biophys. Chem. 162*, 1−5.
(51) Chen, S., Berthelier, V., Yang, W., and Wetzel, R. (2001) Polyglutamine aggregation behavior in vitro supports a recruitment mechanism of cytotoxicity. *J. Mol. Biol. 311*, 173−182.
(52) Chen, S., and Wetzel, R. (2001) Solubilization and disaggregation of polyglutamine peptides. *Protein Sci. 10*, 887−891.
(53) Sharma, D., Sharma, S., Pasha, S., and Brahmachari, S. K. (1999) Peptide models for inherited neurodegenerative disorders: Conformation and aggregation properties of long polyglutamine peptides with and without interruptions. *FEBS Lett. 456*, 181−185.
(54) Chen, S. M., Ferrone, F. A., and Wetzel, R. (2002) Huntington's disease age-of-onset linked to polyglutamine aggregation nucleation. *Proc. Natl. Acad. Sci. U.S.A. 99*, 11884−11889.
(55) Crick, S. L., Jayaraman, M., Frieden, C., Wetzel, R., and Pappu, R. V. (2006) Fluorescence correlation spectroscopy shows that monomeric polyglutamine molecules form collapsed structures in aqueous solutions. *Proc. Natl. Acad. Sci. U.S.A. 103*, 16764−16769.
(56) Masino, L., Kelly, G., Leonard, K., Trottier, Y., and Pastore, A. (2002) Solution structure of polyglutamine tracts in GST-polyglutamine fusion proteins. *FEBS Lett. 513*, 267−272.
(57) Walters, R. H., and Murphy, R. M. (2009) Examing polyglutamine peptide length: A connection between collapsed conformations and increased aggregation. *J. Mol. Biol. 393*, 978−992.